

Positional stability of skyrmions in a racetrack memory with notched geometry

Md Golam Morshed,^{1, a)} Hamed Vakili,^{2, a)} and Avik W. Ghosh^{1,2}

¹⁾*Department of Electrical and Computer Engineering, University of Virginia, Charlottesville, VA 22904, USA*

²⁾*Department of Physics, University of Virginia, Charlottesville, VA 22904, USA*

(Dated: 21 March 2022)

Magnetic skyrmions are chiral spin textures with attractive features, such as ultra-small size, solitonic nature, and easy mobility with small electrical currents that make them promising as information-carrying bits in low-power, high-density memory, and logic applications. However, it is essential to guarantee the positional stability of skyrmions for reliable information extraction. Using micromagnetic simulations for the minimum energy path (MEP), we compute the energy barriers associated with stabilizing notches along a racetrack. We vary material parameters, specifically, the strength of the chiral Dzyaloshinskii-Moriya interactions (DMI) and the notch geometry to get the optimal barrier height. We find that the reduction of skyrmion size as it squeezes past the notch gives rise to the energy barrier. We find a range of energy barriers up to $\sim 45 k_B T$ for a racetrack of 6 nm thickness that can provide year long positional lifetime of skyrmions for long-term memory applications, while requiring a moderate amount of current ($\sim 10^{10}$ A/m²) to move the skyrmions. Furthermore, we derive quasi-analytical equations to estimate the maximum energy barrier. We also explore other pinning mechanisms, such as a local variation of material parameters in a region, and find that notched geometry provides the highest energy barrier. Our results open up possibilities to design practical skyrmion-based racetrack geometries for spintronic applications.

Conventional memory technology is based on digital electronics. It is volatile and severely bottlenecked by the Von Neumann limit - the delay in fetching instruction sets between the logic cores and the memory elements that are slower to scale. The ever-increasing volume of data requires compact high-density integrated circuits where Moore's law is unable to cope with the increasing scaling requirements. Chiral spin textures such as magnetic skyrmions¹⁻³ bear non-trivial properties, such as topological protection⁴, ultra-small size⁵, high-speed⁶, current-induced solitonic motion including nucleation and annihilation^{7,8}. As a result, they have emerged as potential candidates for both digital and analog information-carrying bits in low-power high-density, fast, all-electronic non-volatile memory, and logic applications⁹⁻¹⁵. Magnetic skyrmions originate and stabilize by the chiral Dzyaloshinskii-Moriya interaction (DMI)^{16,17} in systems lacking inversion symmetry, while tuning the DMI¹⁸⁻²¹ controls the skyrmion size²² and overall stability.

Racetrack memory²³ is one of the common platforms studied in the context of skyrmionics^{11,24,25}. In a skyrmion-based Boolean racetrack memory, information can be encoded by the presence (bit "1") and absence (bit "0") of skyrmions at a particular position in the racetrack. For an analog domain utilization of a skyrmion racetrack, such as a native temporal memory for race logic¹¹, the information is encoded directly into the spatial coordinates of the skyrmions, which then can be translated back into the timing information of wavefront

duty cycles carrying out the race logic operations²⁶. The positional stability of skyrmions is a critical issue for both of these applications, as a randomly displaced skyrmion can alter the sequence of the "0" and "1" bits in Boolean memory applications. Similarly, for race logic applications, the displacement of skyrmions would change the spatial coordinates of the skyrmion and hence the encoded analog timings. For reliable information extraction, it is essential to guarantee the positional stability of skyrmions for a certain amount of time. For example, for a long-term memory application it would require positional stability of years, while for cache memory, hours or even minutes would be sufficient. In an ideal racetrack, skyrmions are susceptible to thermal fluctuations and exhibit Brownian motion that leads to the diffusive displacement of skyrmions^{27,28}. Moreover, skyrmions show inertia-driven drift shortly after a current pulse is removed rather than stopping immediately. One way to control such undesirable motion is by engineering confinement barriers such as defects created by local variation of material parameters and notches etched into the racetrack, which ensures the pinning of skyrmions^{7,29}.

The interactions and dynamics of skyrmions with defects and other pinning sites have been studied over the past few years²⁹⁻³². Few of the studies have discussed the energy barrier associated with the pinning sites peripherally^{33,34}. Recently, notches have been used to achieve positional stability in domain wall-based artificial synapses, and they improve the linearity and repeatability of synaptic updates³⁵. Nonetheless, what is missing is a systematic analysis of a notched racetrack, the mechanics of the energy barrier and its impact on skyrmion mobility, stability, and unintended nucleation and annihilation which sets its operating limits. The combination of required positional stability and operational current range defines

^{a)}Authors to whom correspondence should be addressed: mm8by@virginia.edu; hv8rf@virginia.edu; These two authors contributed equally.

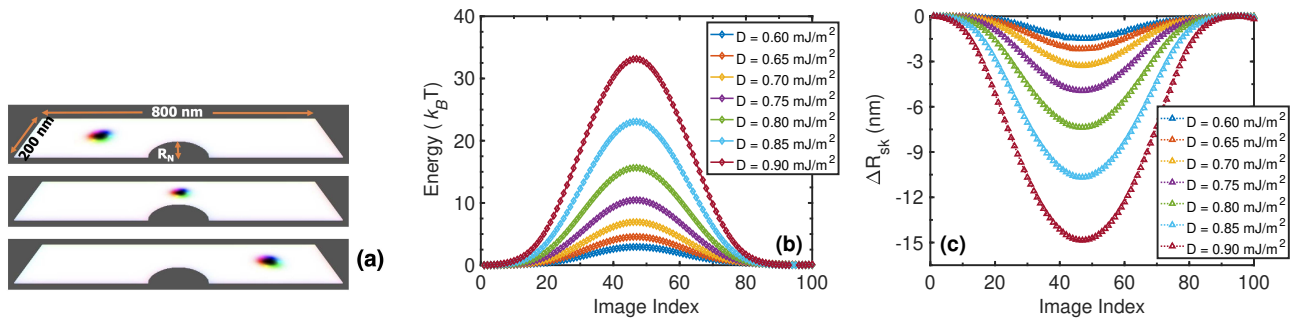


FIG. 1. (a) Schematic of the simulated racetrack with notched geometry. Each of the figures represents different snapshots of the skyrmion trajectory along the racetrack, referred to as ‘image index’. (b) The energy vs image index for the optimal trajectory obtained from MEP calculations of a skyrmion with varying DMIs in a $800\text{ nm} \times 200\text{ nm}$ racetrack with notch radius $R_N = 75\text{ nm}$. The left valley, peak and right valley correspond to the image index showed in the top, middle and bottom panels of Fig. 1(a) respectively. (c) Change in skyrmion radius, ΔR_{sk} when the skyrmion passes over the notch. Higher DMIs initiate larger initial skyrmions that undergo bigger shrinkage and larger energy costs when forced through the constriction.

an optimal ‘Goldilocks’ regime in parameter phase space, which is the focus of this work.

In this letter, we show a systematic analysis of our ability to produce and tune the energy barrier in a skyrmion-based racetrack with notched geometry (Fig. 1) using micromagnetic simulations. In particular, we vary the material parameters DMI (varying skyrmion sizes), the geometry of the notches (Fig. 2a), and thickness of the racetrack (Fig. 2c) to achieve a high tunability of the energy barrier for long-term positional stability of skyrmions. We demonstrate that the energy barrier is attributed to the constriction in the skyrmion sizes arising from the notch created in the racetrack. Additionally, we come up with an empirical equation based on our simulated data (Fig. 3). Furthermore, we explain and compare our simulated data with the analytical energy equations of skyrmions on an unconfined infinite plane plus a phenomenological confinement correction that match perfectly (Fig. 4a). The quantitative difference between the energy of skyrmions on an unconfined infinite plane and our simulated data is attributed to the different geometric boundary conditions (Fig. 4b). We also explore other pinning sites such as local variation of material parameters to put the notched geometry into perspective with other types of defects (Fig. 5). Finally, we show that the required unpinning current is small enough for skyrmion based devices to be integrated with electrical circuits (Fig. 6). Our results provide a path forward towards practical, reliable skyrmion-based racetrack memory applications.

We perform the simulations using MuMax3, a micromagnetics simulator³⁶ that solves the Landau–Lifshitz–Gilbert (LLG) equation. The dimensions of the racetrack are $L = 800\text{ nm}$, $W = 200\text{ nm}$, $t_F = 3\text{ nm}$, and the simulation mesh is divided into $400 \times 100 \times 1$ grids with a cell size of $2\text{ nm} \times 2\text{ nm} \times 3\text{ nm}$ without considering periodic boundary condition. We use material parameters as exchange stiffness $A_{ex} = 12\text{ pJ/m}$, anisotropy $K_u = 50\text{ kJ/m}^3$, saturation magnetization

$M_s = 100\text{ kA/m}$ throughout all the calculations unless otherwise specified. We use varying DMI to control the size of skyrmions because the DMI can be easily tuned by interface engineering^{19,20}. We calculate the minimum energy path (MEP) using the String method^{37,38}. The basic idea of the string method is to find the transition path by evolving a curve (string) connecting two endpoints along the energy landscape and the reparametrization of the string by interpolation^{37,38}. It is an iterative method that continues until the path converges to the MEP with the desired accuracy. In our simulations, we use 100 iterations to calculate the MEP.

Figure 1(a) shows the schematic of the racetrack with notched geometry used for the simulations. We create the semi-circular notch of varying sizes (radius R_N) by removing materials from that particular region of the racetrack. The snapshots represent different positions of the skyrmion trajectory (referred as ‘image index’) along the racetrack as it moves from one side to the other side of the notch. Figure 1(b) shows the total energy obtained from the MEP calculations for a racetrack with a semi-circular notch of radius 75 nm and thickness 3 nm (recall the racetrack width is 200 nm). The zero for energy is set as the energy of the first image index in the simulation domain shown in Fig. 1(a) top. We vary the material parameter DMI, D from 0.60 mJ/m^2 to 0.90 mJ/m^2 and find a maximum energy barrier ranges from ~ 2 to $35\text{ k}_B T$. We find that the energy barrier results from the change in the skyrmion radius, ΔR_{sk} as the skyrmion passes past the notch. We conjecture that the reduction of the skyrmion size in squeezing through the constriction gives rise to the energy barrier.

Figure 1(c) shows the series of ΔR_{sk} of the skyrmion corresponding to the energy plots shown in Fig. 1(b). As the D increases, for a specific exchange and anisotropy, the skyrmion size gets bigger, making it harder to squeeze through and generating a higher energy barrier. The positional lifetime of the skyrmion is often described using an Arrhenius form $\tau = f_0^{-1} e^{E_b/k_B T}$ where f_0 is the at-

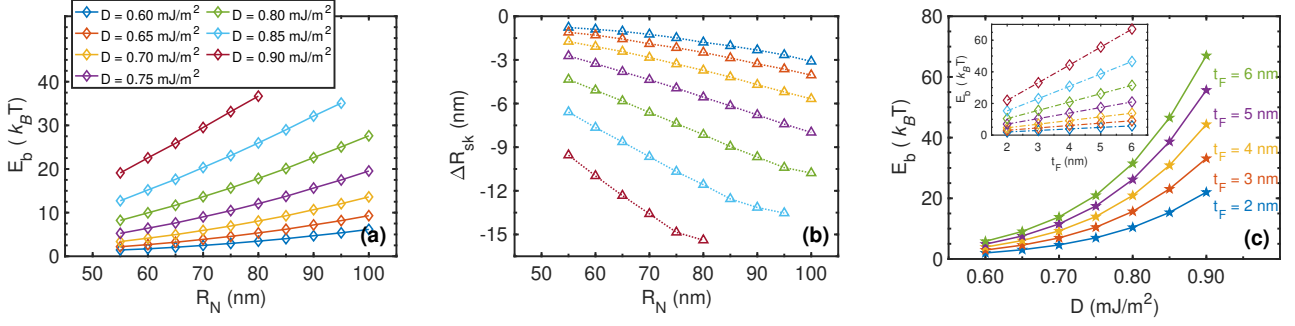


FIG. 2. Material parameter dependence of the maximum energy barrier, E_b . Effect of notch size (radius R_N) on (a) maximum energy barrier, and (b) Change in skyrmion radius, ΔR_{sk} vs R_N , both for varying DMIs. We see that a larger $|\Delta R_{sk}|$ corresponds to a higher barrier. (c) Thickness dependence of the maximum energy barrier in a racetrack with $R_N = 75$ nm. The inset shows that the maximum energy barrier increases linearly as a function of racetrack thickness, t_F for any specific D . The linear variation of E_b vs thickness is consistent with the overall uniform cylindrical shape of the skyrmion at ultrathin limit. The color code to represent DMI variations in (a), (b), and inset of (c) are the same.

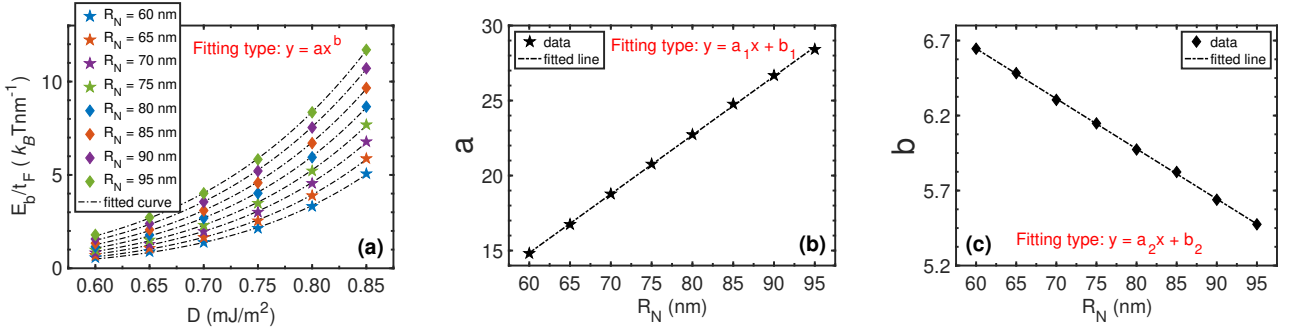


FIG. 3. (a) Fitting of the maximum energy barrier (normalized by the thickness of the racetrack) with respect to the DMI. (b), (c) The relation between the fitting constants obtained from (a) and the notch sizes. The red colored texts in each graph represent the fitting function.

tempt frequency and E_b is the height of the gaussian energy profile. Approximately an E_b of $30 k_B T$ will result in positional lifetime of seconds for an attempt frequency f_0 of 10^{10} Hz. $35 k_B T$ energy barrier will give a lifetime in day.

We calculate the MEP for a series of notch sizes ($R_N = 55 - 100$ nm) and demonstrate the impact on the maximum energy barrier in Fig. 2(a). We find that for all the DMIs, the maximum energy barrier increases as the notch radius increases, by reducing the size of the skyrmion, consistent with Fig. 2(b). As R_N increases, the skyrmion size shrinks more, $|\Delta R_{sk}|$ gets larger, and the energy barrier increases proportionally. However, if we continue to increase R_N , at some point, the skyrmion starts annihilating as the region over the notch is not sufficient enough to pass through and the skyrmion touches the boundary of the notch and the edge of the simulation box. For instance, from Fig. 2(a), we can see that throughout the range of the DMIs ($D = 0.60 - 0.90$ mJ/m²), skyrmions pass through without annihilation up to a notch radius of 80 nm. For larger notches, for example 90 nm and 100 nm, the skyrmion gets annihilated when D is greater than 0.85 mJ/m² and

0.80 mJ/m² respectively.

We also vary another important geometrical parameter, the thickness t_F of the racetrack for a range of DMIs, and find an increase in maximum barrier height for a thicker racetrack for a specific D . Figure 2(c) shows the thickness dependence of the skyrmions in a racetrack with $R_N = 75$ nm for various DMIs. We get a maximum energy barrier of $\sim 45 k_B T$ for a moderately thick (6 nm) racetrack when the skyrmion radius is ~ 35 nm ($D = 0.85$ mJ/m²). According to the positional lifetime equation mentioned above, $45 k_B T$ energy barrier will give years long lifetime that makes this device suitable for long-term storage class memory applications. Obviously, we will get even higher energy barrier for higher notch radius. The inset shows the linearity of the maximum energy barrier as a function of t_F , which dictates that we can increase the energy barrier even further by increasing the thickness of the racetrack.

To quantify the maximum energy barrier E_b , combining all the data we get by varying the D , R_N , and t_F , we come up with a fitted empirical equation, normalized by the thickness of the racetrack. We use a power law fitting to find the relation between the E_b and D . From

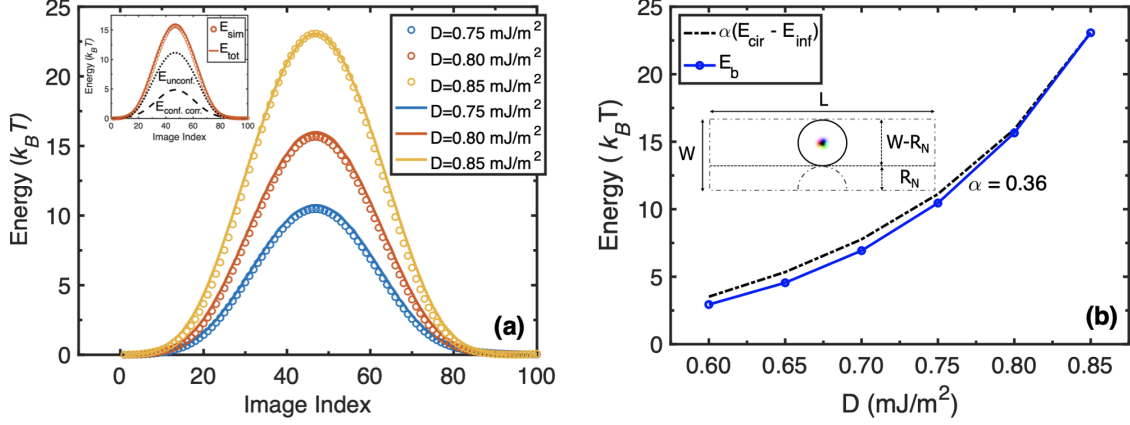


FIG. 4. (a) Energy landscape of skyrmions in a racetrack ($R_N = 75 \text{ nm}$) from the MEP simulations (scatter circles) and analytical equations (solid curves)^{10,39}. The analytical equations include the energetics of 2π skyrmions on an infinite plane plus a phenomenological confinement correction. (b) Explanation of the mismatch between simulated and analytical (calculated using equation 2) data in a racetrack ($R_N = 75 \text{ nm}$). A skyrmion confined above the pinning site has the energy of a skyrmion confined in a circle of diameter $W - R_N$ above the notch minus that of an unconfined infinite plane skyrmion. Including only one fitting term the energy barrier can be described with good accuracy for varying DMI values. The black circular region above the semicircular notch in the inset schematic represents the simulation geometry for the confined case.

Fig. 3(a), we can see that the simulated data for all the R_N values are perfectly described by a power law. The coefficient and exponent are found to be linear functions of the notch radius R_N , as shown in Fig. 3(b) and 3(c). The final form of the empirical equation is

$$E_b/t_F = (0.4R_N - 8.7)D^{-0.03R_N} + 8.7 \quad (1)$$

where the prefactor constants are material specific. The units of E_b , t_F , D , and R_N are in $k_B T$, nm , mJ/m^2 , and nm respectively. As energy of skyrmion increases linearly with thickness for the limit of uniform cylindrical shape of skyrmion (inset of Fig. 3(c)) at the limit of ultrathin films ($\lesssim 10 \text{ nm}$), the thickness t_F is simply a scaling factor. We note that the above equation holds for $R_N > 0$ and we get $E_b = 0$ when $R_N = 0$.

We compare our simulated data with the analytical equation derived for skyrmions^{10,39}. The different energy terms that give total energy equation of the skyrmions on an infinite plane are derived as^{10,39}

$$\begin{aligned} E_{\text{ex}} &= (2\pi A_{\text{ex}} t_F) \left(\frac{2R_{\text{sk}}}{\Delta} + \frac{2\Delta}{R_{\text{sk}}} N_{\text{sk}}^2 \right) f_{\text{ex}}(\rho) \\ E_{\text{DMI}} &= -(2\pi R_{\text{sk}} t_F) \pi D f_{\text{DMI}}(\rho) \\ E_{\text{ani}} &= (4\pi K_u t_F) R_{\text{sk}} \Delta f_{\text{ani}}(\rho) \end{aligned} \quad (2)$$

where R_{sk} , Δ , N_{sk} are skyrmion radius, domain wall width, and skyrmion winding number respectively. The form factors for small size, obtained by fitting numerical

simulations, are given by^{10,39}

$$\begin{aligned} f_{\text{ex}}(\rho) &\approx \left[1 + 1.93 \frac{\rho(\rho - 0.65)}{\rho^2 + 1} e^{-1.48(\rho - 0.65)} \right] \\ f_{\text{ani}}(\rho) &\approx \left[1 - \frac{1}{6\rho} e^{-\rho/\sqrt{2}} \right] \\ f_{\text{DMI}}(\rho) &\approx \left[N_{\text{sk}} + \frac{1}{2\pi\rho} e^{-\rho} \right] \end{aligned} \quad (3)$$

where $\rho = R_{\text{sk}}/\Delta$. Figure 4(a) shows that our simulated energy profiles (scattered circles) are perfectly matched with the analytical equation (solid curves) that includes the energetics of skyrmions within 2π model on an infinite plane $E_{\text{unconf.}} = E_{\text{ex}} + E_{\text{DMI}} + E_{\text{ani}}$, plus a phenomenological confinement correction $E_{\text{conf. corr.}}$ (see the dotted and dashed black curves in the inset of Fig. 4(a) for $E_{\text{unconf.}}$ and $E_{\text{conf. corr.}}$ respectively; adding up these two curves give the $E_{\text{tot.}}$). We use gaussian fitting to derive $E_{\text{conf. corr.}}$ that can be expressed as

$$E_{\text{conf. corr.}} = A e^{-\left(\frac{x-B}{C}\right)^2} \quad (4)$$

where A is the magnitude of the curve, $B = 47$, $C = 20$, and x is a placeholder for ‘image index’. A is a quadratic

function of D and R_N , and can be expressed as

$$A = [A_0 + \frac{(D - D_{min})^2}{(0.90 - D_{min})^2}]k_B T$$

$$A_0 = 3 + \frac{4(R_N^2 - 60^2)}{90^2 - 60^2}$$

$$D_{min} = 0.75 + \frac{|R_N - 60|}{1000} \quad (5)$$

We note that we use $N_{sk} = 1$ and the value of R_{sk} and Δ obtained from micromagnetic simulations while calculating the energy from the equation (2). However, equation (2) alone fails to capture the simulated energy profiles because of the fact that it assumes an unconfined planar geometry while in our simulations, we use a confined geometry. We conjecture that our simulated maximum energy barrier will be somewhere in between the skyrmion energy on an unconfined infinite plane and that for a confined circular region around the notch. To verify, we calculate the static energy of skyrmions both for a circle (E_{cir}) above the notch region with diameter $W - R_N$ (see the inset of Fig. 4(b)), and for an unconfined infinite plane (E_{inf}). In Fig. 4(b), we show the energy difference between E_{cir} and E_{inf} for a racetrack with $R_N = 75 \text{ nm}$. We find that the our simulated E_b matches with $\alpha(E_{cir} - E_{inf})$ for the the entire range of D , where α is a prefactor dependent on the racetrack geometry. We compare $\alpha(E_{cir} - E_{inf})$ and E_b for other notch radii and find overall agreement, while α varies as a function of notch radius.

We explore alternate pinning mechanisms to compare the maximum energy barrier among them. One common approach to introduce pinning sites is a local variation of the material parameters in a specific region in the racetrack^{7,29}. In practical systems, the variation of material parameters can be achieved by naturally occurring and intentional defects, grain boundaries, composition and thickness gradient in the thin films, voltage gating, modulating the heavy metal layer, etc. We create the pinning sites by locally varying anisotropy K_u , exchange stiffness A_{ex} , DMI D , and saturation magnetization M_s . We vary one parameter at a time while the other parameters remain constant throughout the racetrack. Figure 5(a) shows the maximum energy barrier for different pinning sites, including the fully notched geometry for a 3 nm thick racetrack having a semi-circular pinning site of 75 nm radius. It appears that a fully notched geometry racetrack produces highest maximum energy barrier than the rest, which attributes to the largest change in skyrmion radius while passing over the notch as shown in Fig. 5(b). Additionally, notches are easier to create experimentally than controlling the local variation of material parameters.

We also calculate the maximum energy barrier for two promising materials (GdCo and Mn₄N) for skyrmion-based spintronics applications^{40,41}. GdCo and Mn₄N are ferrimagnets and are found to be attractive for hosting

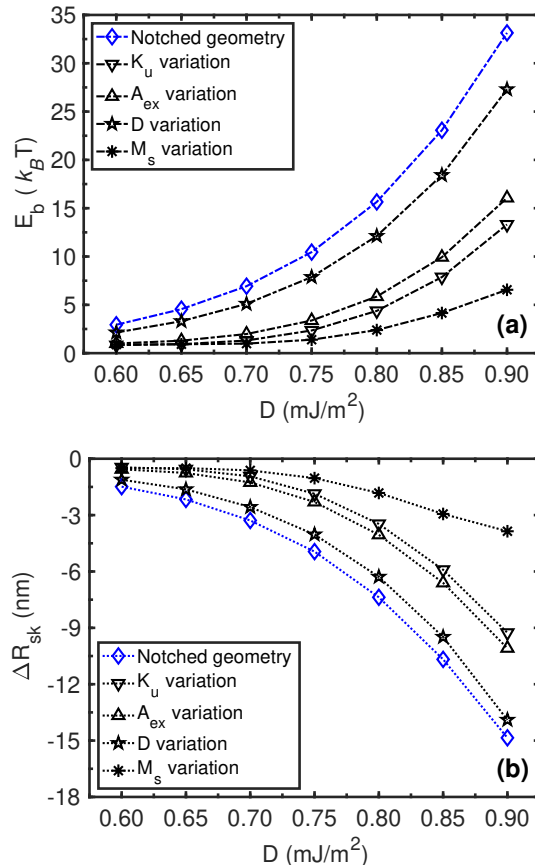


FIG. 5. (a) Maximum energy barrier for different pinning sites in a 3 nm thick racetrack. For all the cases, the pinning site is a semi-circular region of 75 nm radius. The anisotropy, K_u and exchange stiffness, A_{ex} of the pinning site are 2 times higher, and the DMI, D and saturation magnetization, M_s are 10 times lower than the rest of the track region. We choose the ratio that gives highest maximum energy barrier. (b) Change in skyrmion radius, ΔR_{sk} corresponding the energy barrier in (a), shows a proportional relation between E_b and $|\Delta R_{sk}|$.

small and speedy skyrmions. In a 3 nm thick racetrack ($R_N = 75 \text{ nm}$), for a $\sim 40 \text{ nm}$ skyrmion, we find an energy barrier of $\sim 12 k_B T$ and $\sim 25 k_B T$ for GdCo and Mn₄N, respectively (parameters of GdCo and Mn₄N are taken from the literature^{5,10,39,42}). Our finding suggests that Mn₄N offers a higher energy barrier than GdCo, which is mainly because of the higher exchange stiffness of Mn₄N. Needless to say that the energy barrier can be further increased by playing with the notch radius and thickness of the racetrack.

While a barrier is needed to hold the skyrmion in place, it is equally important to ensure that the critical current to depin the skyrmions is not too large, as that would cause unacceptable energy dissipation when integrated with the peripheral circuitry, not to mention random skyrmion annihilation, and even occasional unintended nucleation⁴³. The energy barrier can be tuned by varying various knobs such as materials parameters and notch

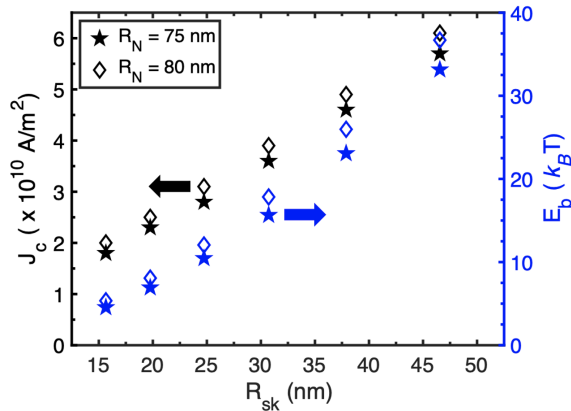


FIG. 6. The critical current J_c (black) to unpin the skyrmion and the corresponding energy barrier (blue) for a 3 nm thick racetrack having notch radius R_N as a function of skyrmion size. We see a low unpinning current with a fairly large energy barrier. The arrows point each colored data to the corresponding y -axis.

geometries. However, it needs to be optimized so it provides a high enough hold time for the skyrmions yet requires a moderate unpinning current.

In Fig. 6, we show the unpinning current of racetracks with 75 nm and 80 nm notch radii, and 3 nm thickness. The current density distribution for the racetrack with the notch is calculated using COMSOL Multiphysics®⁴⁴. We use current pulses ranging from 5 ns to 20 ns to unpin the skyrmions. We find that bigger skyrmions need a shorter pulse, and the critical current increases as energy barrier increases. The energy barrier increases faster with radius than the critical current, which would help us get a large enough barrier and a small enough unpinning current. We find a moderate critical current for a large energy barrier. For instance, a ~ 45 nm skyrmion can be uninned with a current of 6.1×10^{10} A/m² while the corresponding energy barrier is ~ 35 $k_B T$. We also calculate the critical current for thicker racetracks that provide much a higher energy barrier. For example, for 5 nm and 6 nm racetracks ($R_N = 75$ nm), a ~ 35 nm skyrmion (corresponding energy barriers are ~ 40 $k_B T$ and ~ 45 $k_B T$) can be uninned with a current pulse of 7.5×10^{10} A/m² and 9.0×10^{10} A/m² respectively, which are orders of magnitude smaller than the critical current required to unpin domain walls^{23,45}. Moreover, the obtained critical currents are significantly lower than the nucleation current ($> 10^{12}$ A/m²) of the skyrmions in a constricted geometry^{43,46}, which prevents any unintended nucleation of skyrmions during the unpinning process.

In summary, we demonstrated that skyrmion positional stability is achievable by creating notches along a racetrack. We presented quantitative analyses, backed by analytical equations for various material parameters, notch geometries and racetrack thicknesses. An optimal combination of skyrmion size, notch radius, and thick-

ness of the racetrack provides a large enough energy barrier (~ 45 $k_B T$) to achieve a positional lifetime of years for long-term memory applications. We found a moderately low minimum critical current to unpin the skyrmion ($\sim 10^{10}$ A/m²), which is an essential aspect for low-power operations. These results provide critical design insights on skyrmionic racetracks, and potentially an argument for reliable, long-term skyrmion-based memory applications.

ACKNOWLEDGMENTS

This work is funded by the DARPA Topological Excitations in Electronics (TEE) program (grant D18AP00009). The calculations are done using the computational resources from High-Performance Computing systems at the University of Virginia (Rivanna) and XSEDE. We thank Mark Stiles, Andrew Kent, Prasanna Balachandran, Mircea Stan, Geoffrey Beach and Joe Poon for useful discussions.

DATA AVAILABILITY

The data that support the findings of this study are available from the corresponding author upon reasonable request.

REFERENCES

- S. Mühlbauer, B. Binz, F. Jonietz, C. Pfleiderer, A. Rosch, A. Neubauer, R. Georgii, and P. Böni, *Science* **323**, 915 (2009).
- S. Heinze, K. von Bergmann, M. Menzel, J. Brede, A. Kubetzka, R. Wiesendanger, G. Bihlmayer, and S. Blügel, *Nat. Phys.* **7**, 713 (2011).
- H. Vakili, Y. Xie, and A. W. Ghosh, *Phys. Rev. B* **102**, 174420 (2020).
- S.-G. Je, H.-S. Han, S. K. Kim, S. A. Montoya, W. Chao, I.-S. Hong, E. E. Fullerton, K.-S. Lee, K.-J. Lee, M.-Y. Im, and J.-I. Hong, *ACS Nano* **14**, 3251 (2020).
- L. Caretta, M. Mann, F. Büttner, K. Ueda, B. Pfau, C. M. Günther, P. Helsing, A. Churikova, C. Klose, M. Schneider, D. Engel, C. Marcus, D. Bono, K. Bagschik, S. Eisebitt, and G. S. D. Beach, *Nat. Nanotechnol.* **13**, 1154 (2018).
- Y. Liu, N. Lei, C. Wang, X. Zhang, W. Kang, D. Zhu, Y. Zhou, X. Liu, Y. Zhang, and W. Zhao, *Phys. Rev. Appl.* **11**, 014004 (2019).
- J. Sampaio, V. Cros, S. Rohart, A. Thiaville, and A. Fert, *Nat. Nanotechnol.* **8**, 839 (2013).
- N. Romming, C. Hanneken, M. Menzel, J. E. Bickel, B. Wolter, K. von Bergmann, A. Kubetzka, and R. Wiesendanger, *Science* **341**, 636 (2013).
- A. Fert, N. Reyren, and V. Cros, *Nat. Rev. Mater.* **2**, 1 (2017).
- H. Vakili, J.-W. Xu, W. Zhou, M. N. Sakib, M. G. Morshed, T. Hartnett, Y. Quessab, K. Litzius, C. T. Ma, S. Ganguly, M. R. Stan, P. V. Balachandran, G. S. D. Beach, S. J. Poon, A. D. Kent, and A. W. Ghosh, *J. Appl. Phys.* **130**, 070908 (2021).
- H. Vakili, M. N. Sakib, S. Ganguly, M. Stan, M. W. Daniels, A. Madhavan, M. D. Stiles, and A. W. Ghosh, *IEEE J. Explor. Solid-State Comput. Devices Circuits* **6**, 107 (2020).
- M. N. Sakib, H. Vakili, S. Ganguly, S. Mosanu, A. W. Ghosh, and M. Stan, in *Spintronics XIII*, Vol. 11470 (International Society for Optics and Photonics, 2020) p. 114703D.
- S. Luo, M. Song, X. Li, Y. Zhang, J. Hong, X. Yang, X. Zou, N. Xu, and L. You, *Nano Lett.* **18**, 1180 (2018).

- ¹⁴M. G. Mankalale, Z. Zhao, J.-P. Wang, and S. S. Sapatnekar, *IEEE Trans. Electron Devices* **66**, 1990 (2019).
- ¹⁵S. Luo and L. You, *APL Mater.* **9**, 050901 (2021).
- ¹⁶I. Dzyaloshinsky, *J. Phys. Chem. Solids* **4**, 241 (1958).
- ¹⁷T. Moriya, *Phys. Rev.* **120**, 91 (1960).
- ¹⁸H. Yang, A. Thiaville, S. Rohart, A. Fert, and M. Chshiev, *Phys. Rev. Lett.* **115**, 267210 (2015).
- ¹⁹Y. Quessab, J.-W. Xu, C. T. Ma, W. Zhou, G. A. Riley, J. M. Shaw, H. T. Nembach, S. J. Poon, and A. D. Kent, *Sci. Rep.* **10**, 1 (2020).
- ²⁰M. G. Morshed, K. H. Khoo, Y. Quessab, J.-W. Xu, R. Laskowski, P. V. Balachandran, A. D. Kent, and A. W. Ghosh, *Phys. Rev. B* **103**, 174414 (2021).
- ²¹Y. Quessab, J.-W. Xu, M. G. Morshed, A. W. Ghosh, and A. D. Kent, *Adv. Sci.* **8**, 2100481 (2021).
- ²²X. S. Wang, H. Y. Yuan, and X. R. Wang, *Commun. Phys.* **1**, 1 (2018).
- ²³S. S. P. Parkin, M. Hayashi, and L. Thomas, *Science* **320**, 190 (2008).
- ²⁴A. Fert, V. Cros, and J. Sampaio, *Nat. Nanotechnol.* **8**, 152 (2013).
- ²⁵R. Tomasello, E. Martinez, R. Zivieri, L. Torres, M. Carpentieri, and G. Finocchio, *Sci. Rep.* **4**, 1 (2014).
- ²⁶A. Madhavan, T. Sherwood, and D. Strukov, in *ACM SIGARCH Computer Architecture News*, Vol. 42 (Association for Computing Machinery, New York, NY, USA, 2014) pp. 517–528.
- ²⁷D. Cortés-Ortuño, W. Wang, M. Beg, R. A. Pepper, M.-A. Bisotti, R. Carey, M. Vousden, T. Kluyver, O. Hovorka, and H. Fangohr, *Sci. Rep.* **7**, 1 (2017).
- ²⁸L. Zhao, Z. Wang, X. Zhang, X. Liang, J. Xia, K. Wu, H.-A. Zhou, Y. Dong, G. Yu, K. L. Wang, X. Liu, Y. Zhou, and W. Jiang, *Phys. Rev. Lett.* **125**, 027206 (2020).
- ²⁹Y.-H. Liu and Y.-Q. Li, *J. Phys.: Condens. Matter* **25**, 076005 (2013).
- ³⁰J. Müller and A. Rosch, *Phys. Rev. B* **91**, 054410 (2015).
- ³¹H. C. Choi, S.-Z. Lin, and J.-X. Zhu, *Phys. Rev. B* **93**, 115112 (2016).
- ³²C. Reichhardt, C. J. O. Reichhardt, and M. V. Milosevic, *arXiv* (2021), 2102.10464.
- ³³D. Cortés-Ortuño, W. Wang, M. Beg, R. A. Pepper, M.-A. Bisotti, R. Carey, M. Vousden, T. Kluyver, O. Hovorka, and H. Fangohr, *Scientific Reports* **7**, 4060 (2017).
- ³⁴D. Suess, C. Vogler, F. Bruckner, P. Heistracher, F. Slanovc, and C. Abert, *Sci. Rep.* **9**, 1 (2019).
- ³⁵S. Liu, T. P. Xiao, C. Cui, J. A. C. Incorvia, C. H. Bennett, and M. J. Marinella, *Appl. Phys. Lett.* **118**, 202405 (2021).
- ³⁶A. Vansteenkiste, J. Leliaert, M. Dvornik, M. Helsen, F. Garcia-Sanchez, and B. Van Waeyenberge, *AIP Adv.* **4**, 107133 (2014).
- ³⁷W. E, W. Ren, and E. Vanden-Eijnden, *Phys. Rev. B* **66**, 052301 (2002).
- ³⁸W. E, W. Ren, and E. Vanden-Eijnden, *J. Chem. Phys.* **126**, 164103 (2007).
- ³⁹F. Büttner, I. Lemesch, and G. S. D. Beach, *Sci. Rep.* **8**, 1 (2018).
- ⁴⁰C. T. Ma, Y. Xie, H. Sheng, A. W. Ghosh, and S. J. Poon, *Sci. Rep.* **9**, 1 (2019).
- ⁴¹W. Zhou, C. T. Ma, T. Q. Hartnett, P. V. Balachandran, and S. J. Poon, *AIP Adv.* **11**, 015334 (2021).
- ⁴²T. Gushi, L. Vila, O. Fruchart, A. Marty, S. Pizzini, J. Vogel, F. Takata, A. Anzai, K. Toko, T. Suemasu, and J.-P. Attané, *arXiv* (2018), 10.7567/JJAP.57.120310, 1810.13184.
- ⁴³F. Büttner, I. Lemesch, M. Schneider, B. Pfau, C. M. Günther, P. Hessing, J. Geilhufe, L. Caretta, D. Engel, B. Krüger, J. Viehhaus, S. Eisebitt, and G. S. D. Beach, *Nat. Nanotechnol.* **12**, 1040 (2017).
- ⁴⁴COMSOL Multiphysics® v. 5.6. www.comsol.com. COMSOL AB, Stockholm, Sweden.
- ⁴⁵T. Gushi, M. Jovičević Klug, J. Peña Garcia, S. Ghosh, J.-P. Attané, H. Okuno, O. Fruchart, J. Vogel, T. Suemasu, S. Pizzini, and L. Vila, *Nano Lett.* **19**, 8716 (2019).
- ⁴⁶J. Iwasaki, M. Mochizuki, and N. Nagaosa, *Nat. Nanotechnol.* **8**, 742 (2013).